heritage

Article

Comparative Study of Architectural Bricks from Khorsabad and Susa Sites: Characterization of Black Glazes

Emmie Beauvoit [1,2,*], Anne Bouquillon [1,2], Odile Majérus [1,2], Daniel Caurant [1,2], Julien Cuny [3] and Ariane Thomas [3]

[1] Centre de Recherche et de Restauration des Musées de France (C2RMF), Palais du Louvre, 14 Quai François Mitterrand, 75001 Paris, France; anne.bouquillon@culture.gouv.fr (A.B.); odile.majerus@chimieparistech.psl.eu (O.M.); daniel.caurant@chimieparistech.psl.eu (D.C.)
[2] Institut de Recherche de Chimie Paris (IRCP), Centre National de la Recherche Scientifique (CNRS), Chimie ParisTech, PSL Research University, 75005 Paris, France
[3] Département des Antiquités Orientales, Musée du Louvre, Porte Mollien, 75001 Paris, France; julien.cuny@louvre.fr (J.C.); ariane.thomas@louvre.fr (A.T.)
* Correspondence: emmie.beauvoit@culture.gouv.fr

Abstract: In this study, the well-preserved glazes of 13 colored bricks representative of the decoration of the palaces of Sargon II (Khorsabad, 8th century BC) and of Darius I (Susa, 6th century BC) were examined. The purpose of this research is to gather information about the ancient brick manufacturing processes by examining the colored glazes and, in particular, black glazes using a combination of methods that included optical microscopy, SEM-EDX, synchrotron µ-XRD, and µ-Raman spectroscopy. The results revealed different coloring techniques for producing black glazes in the Neo-Assyrian and Persian Achaemenid periods. Regarding the black glazes of Susa, it is particularly interesting to note that their chemical composition varies according to the function of the glazes on the bricks: manganese oxide (for colored fields of glaze) and iron-rich compounds (for raised lines separating glazed areas). In comparison, the black glazes from Khorsabad are characterized by the presence of spherical copper sulfide and galena nanoparticles (ranging from less than 100 nm to about 1 µm) for both the glazed areas and the separating lines. This coloring technique to obtain black glazes is very rarely described in the literature, as well as the mechanism of formation of these spherical nanoparticles.

Keywords: architecture; bricks; Susa; Khorsabad; black glazes; nanoparticle; sulfide

Citation: Beauvoit, E.; Bouquillon, A.; Majérus, O.; Caurant, D.; Cuny, J.; Thomas, A. Comparative Study of Architectural Bricks from Khorsabad and Susa Sites: Characterization of Black Glazes. *Heritage* **2023**, *6*, 6291–6310. https://doi.org/10.3390/heritage6090329

Academic Editor: Rafael Fort González

Received: 28 July 2023
Revised: 2 September 2023
Accepted: 6 September 2023
Published: 8 September 2023

1. Introduction

The use of colored glazed bricks characterized the monumental architecture of Middle Eastern palaces and cities between the 14th and 4th centuries BC [1]. The production of this kind of decoration required thorough knowledge and important resources, in a societal context favorable to invention and exchange. The regions of production of these bricks (Assyria, Babylonia, Elam) moved throughout history between the Mesopotamian alluvial plain and the Iranian world [2]. However, the share of knowledge and local innovations that took place in this geographical area are not clearly defined. That is why diachronic investigation is essential in order to refine the evolution of ancient practices and the technological transfers that may have taken place.

More precisely, this research is focused on the comparative study of productions from the Neo-Assyrian (900–610 BC) and Persian Achaemenid (539–330 BC) empires. During this period, glazed bricks adorned the huge cities and palaces of the kings who thus proved their magnificence. Among the various colors of these architectural decorations (different shades of blue, white, black, yellow, orange, green), we concentrated on black glazes that are used to separate different glazes or to fill colored areas. It is noteworthy that it is difficult to objectively identify the color of the black glaze, and in the literature, the different color descriptions included brown, gray, dark blue, dark green or blackish glazes.

Several studies have investigated the different black coloring techniques employed in different chronological periods for the production of glazed bricks in the Middle East [3–8]. A previous paper determined that the black glaze can be colored by copper sulfide nanoparticles distributed throughout the glaze, with a probable contribution of the Fe^{3+}-S^{2-} chromophore [5]. In fact, this sort of pigment seems to have been employed by the Neo-Assyrians from Khorsabad and Aššur and Neo-Babylonians from Babylon for black glazes [5]. The present work aims to further investigate the characterization of these decorations in a larger corpus in order to improve understanding of their production. From the rich collections of the Louvre Museum, two corpora of bricks were selected, including bricks excavated at the archaeological sites of the royal palaces of Sargon II in Dûr-Sharrukin (modern Khorsabad, Iraq) and of Darius I in Susa (Iran) (Figure 1). These ancient cities correspond to two different geographical and chronological periods, which allow us to consider a comparative study of these productions. Khorsabad, formerly Dûr-Sharrukin, was founded in northern Mesopotamia in 713 BC by the Assyrian king Sargon II, who reigned from 721 to 705 BC. The walls of his palace and the royal city were decorated with colored glazed bricks [9,10]. At the death of the king, the city was abandoned, unfinished, by his son Sennacherib. The decorative subjects represented are very diverse, both figurative and geometrical. A wide variety of figures are depicted, as well as animals and mythological creatures. Other abstract and vegetal designs such as bands with geometric and floral patterns framed the friezes and decorated the walls of the palace and public structures. The second corpus of bricks examined concerns the palace built in Susa during the reign of Darius I (522–486 BC), considered the golden age of the Achaemenid Persian Empire. He ruled a territory stretching from the Indus valley to the Balkans and established one of the capitals of his empire at Susa. There, he decided to build a magnificent palace, which was decorated with large ornamental ensembles including the famous life-size Archers' frieze [11,12].

Figure 1. Location of the archaeological sites of Khorsabad and Susa (© d-maps.com, accessed on 23 August 2023).

The purpose of this research is to gather information about the brick manufacturing processes by examining colored glazes using complementary techniques (optical microscopy, SEM-EDS, μ-Raman, and SXRD) to identify both the coloring agents and the chemical composition of the black glazes. The data obtained in the context of this work were compared and recontextualized with available published data on other brick productions. This provides a valuable tool for supporting hypotheses on the development of production techniques used by brick craftsmen in the Middle East in antiquity.

2. Materials and Methods

2.1. Archaeological Bricks

In this study, the well-preserved glazes of some colored bricks representative of the decoration of the Neo-Assyrian and Achaemenid palaces were examined. The archaeological material studied comes from the collections of the Department of Near Eastern Antiquities of the Musée du Louvre. More precisely, seven bricks from the palace of Darius I in Susa (6th century BC) and six bricks from the palace of Sargon II in Khorsabad (8th century BC) were selected (Figure 2a,b). These two corpora of bricks differ from each other in several aspects, as we have just noticed, concerning the period and the place of production. Moreover, the observation and material study of these bricks show significant differences in the recipes of the ceramic bodies. Indeed, most of the Achaemenid Persian bricks from Susa have quartz-based siliceous bodies while the Neo-Assyrian bricks from Khorsabad are made from clay [11,13]. The bricks were chosen according to their state of conservation and the color diversity of the glazes. As a matter of fact, the studied glazed bricks were covered with several colored glazes, including blue, green, yellow, orange, black, and white colors separated by a black glaze. The black glaze is used mainly for two purposes: to outline the patterns, or as flat areas of color (e.g., the checkerboard shown on brick N8098, Figure 2a). Despite the fact that some glazes on the bricks from Susa are particularly weathered, millimetric samples of black glazes were taken from all bricks for our study using a scalpel, avoiding weathered areas.

2.2. Analytical Techniques

Cross-sections of the glazes were prepared to study each sample's microstructure by scanning electron microscopy (SEM), chemical composition with energy-dispersive X-ray spectroscopy (EDS) and mineralogical composition with μ-Raman. Millimeter-sized samples were also directly analyzed by X-ray diffraction at the synchrotron (SXRD). The synchrotron and its particularly intense X-ray beam made it possible to obtain a more intense signal for our microscopic samples.

2.2.1. Scanning Electron Microscopy–Energy-Dispersive X-ray Spectroscopy (SEM-EDS)

The chemical characterization of the brick glazes was determined using a JEOL 7800F scanning electron microscope coupled with two AXS 6/30 energy-dispersive X-ray spectrometers. Samples were coated with platinum and micrographs were recorded in backscattered electron mode (BSE). The resolution of the EDS detector is 129 eV at the Mn-Kα line energy. For the chemical analysis, the experimental conditions were an acceleration voltage of 15 kV using a 1.70 nA electron beam current. The software Esprit (Bruker® Quantax Duo 400, Bruker, Billerica, MA, USA) allowed us to achieve the quantification of the results using the $\varphi(\rho z)$ method. For the quantification of the glass matrices (i.e., the continuous glassy phase surrounding the pigment particles), several areas (at least two) as large as possible (a minimum of 10 μm × 10 μm) were scanned, while the composition of the inclusions was obtained by analysis of small areas or by performing several spot analyses.

2.2.2. Raman Microspectroscopy (μ-Raman)

The mineralogical nature of inclusions in the glazes was identified using μ-Raman spectroscopy. The instrument used is a Renishaw® inVia spectrometer (Renishaw, Wotton-under-Edge, UK), which is equipped with a 532 nm laser, a grating with 1800 L/mm, a

confocal Leica® DM2500 microscope (Leica, Wetzlar, Germany) with four optical objectives (×5, ×20, ×50, ×100), and a CCD detector coupled with the computer system. We shall note that the μ-Raman analysis was performed taking care not to apply too much laser power in order to avoid transformation of the mineralogical composition of the iron-rich inclusions by the incident laser [14]. The wavelength scale at the beginning of each experiment was calibrated using silicon at 520.5 cm^{-1}. The exposure time and the accumulations were adjusted to the fluorescence level and to obtain sufficiently informative spectra. Spikes of cosmic rays and baseline were removed thanks to the software WiRE™ (Renishaw®). Spectra identification was carried out using the RRUFF database on minerals.

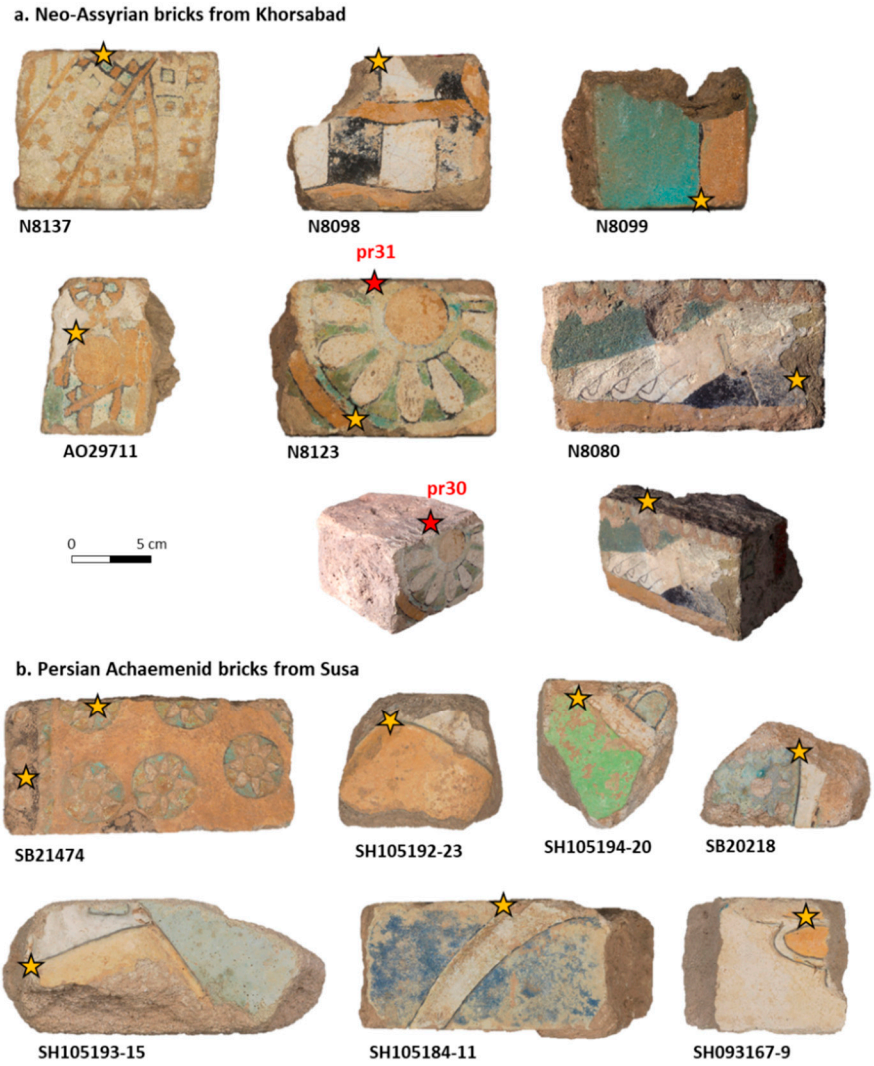

Figure 2. Glazed bricks from the palace of Sargon II in Khorsabad (**a**) and the palace of Darius I in Susa (**b**) (© C2RMF/A. Maigret). Stars indicate the locations of the glazes that were sampled. The two black glazes sampled, pr30 and pr31 (corresponding to red stars), have the peculiarity of not being close to a yellow glaze.

2.2.3. High-Resolution Synchrotron X-ray Diffraction (SXRD)

Moreover, some archaeological samples were also analyzed using high-resolution synchrotron X-ray diffraction analyses performed at the ID22 beamline of the European Synchrotron Radiation Facility (ESRF, Grenoble, France), thanks to the Historical Materials "Block Allocation Group"(BAG) access [15,16]. In the context of the BAG, standardized operating conditions were provided, and the synchrotron X-ray diffraction data were recorded at a wavelength of λ = 0.3542 Å, corresponding to an incident radiation of 35 keV. The micro fragments of glazes were put into borosilicate glass capillaries (0.5 mm in diameter),

which were sealed using wax. All samples were measured under rotation to minimize potential preferred orientation effects. The high-resolution diffraction patterns were collected over the range 1−30° (2θ) in continuous scanning mode (corresponding approximately to an analysis time of 20 min). Throughout the scanning, the capillaries were rotating perpendicular to the X-ray beam of about ~1 × 1 mm^2. The wavelength and the detector parameters were calibrated using a diffraction pattern collected on LaB_6 and Si samples. The identification of the mineralogical phases was performed using QualX software and the database PDF-4+ from the ICDD (International Centre for Diffraction Data).

3. Results

3.1. Susa Glazes

The black glazes on the architectural bricks of the palace of Darius I in Susa can be divided into two different groups: one is used to separate colored glazes and the other is used to achieve the flat color. It is particularly interesting to note that the chemical composition of these two kinds of glazes varies according to their function. Actually, for one brick of the corpus we discerned both a black raised line and a black area (Figure 3a–c). The observation and analysis revealed that the black glazed area is colored at a very fine scale in the bulk, while the black glaze separating other glazes contains a lot of dark inclusions of varying size (between a few microns and several tens of microns in length, Figure 3c).

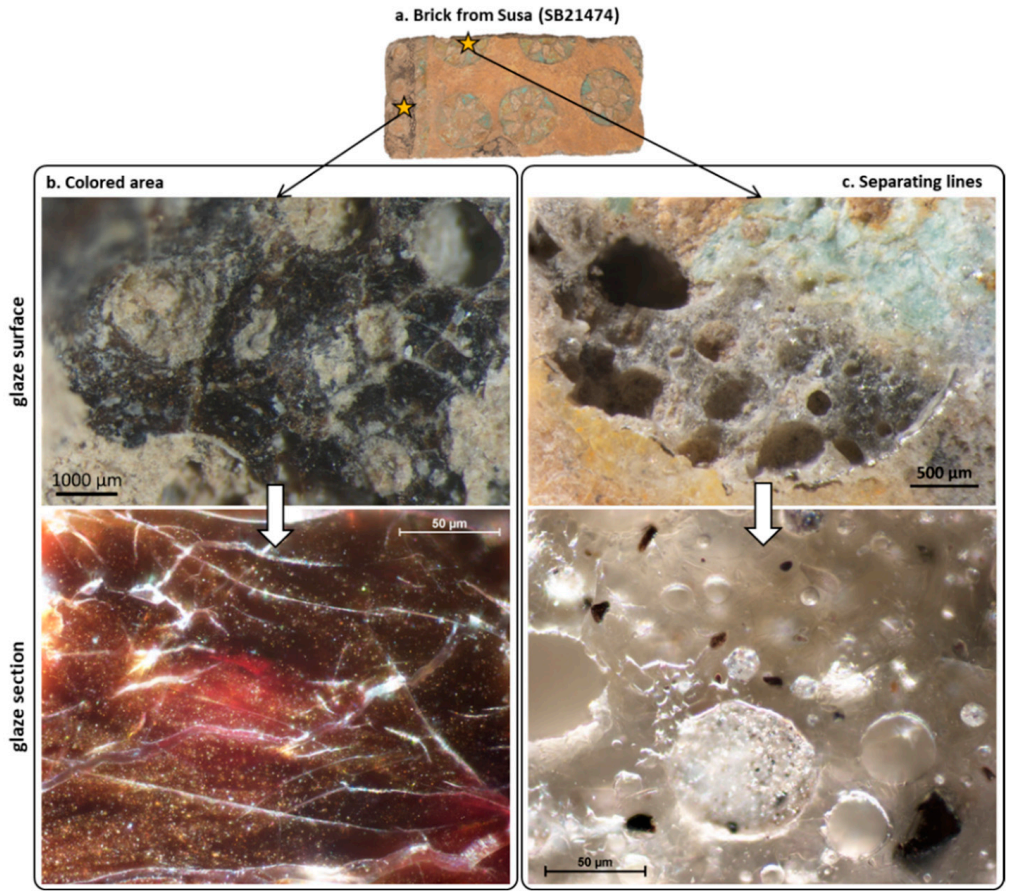

Figure 3. Observation of the surface and the section of the different kind of black glazes present in the same archaeological brick (SB21474, (**a**)) for a black area (**b**) and a dark contour line (**c**).

Firstly, we will develop the characteristics of the glaze used as a colored field. Visually, the glaze appears to be severely degraded, the piece has lost its gloss, and we can see a lot of cracks in the glaze cross-section (Figures 3b and 4a). Supporting our optic observation, EDS analysis showed that the glass matrix is very poor in alkalis (less than 1 wt% Na_2O

and K_2O) and rich in SiO_2 (around 89 wt%). This confirms that the glaze was probably altered and that the alkaline elements were probably leached out during the burial (Table 1). Weathered glazes covering bricks found at Persepolis, Rabat, and Qalaichi (near Hasanlu, 800–600 BC) show a very similar morphology [17]. Due to the very high refractory character of glass compositions so rich in silica, it is very unlikely that glazes with this composition were deposited as glass frits on the bricks with the heating techniques of that time.

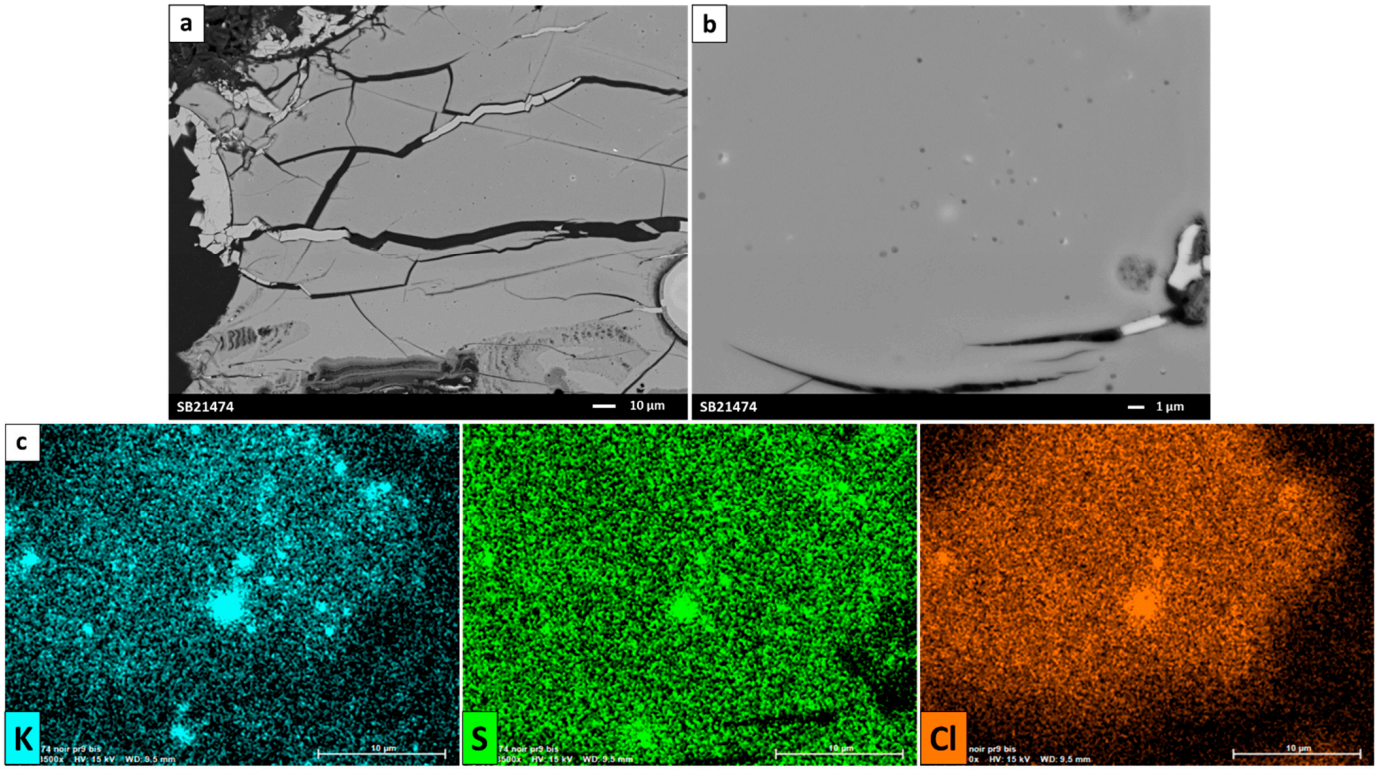

Figure 4. (**a**,**b**) SEM backscattered electron images of the black area (brick SB21474). (**c**) The EDS elemental mappings of the elements K, S, and Cl correspond exactly to the SEM image (**b**). Calcium-rich alteration products are visible in the cracks of the glaze.

Observation by optical microscopy revealed clouds of light spots (less than 1 µm in diameter) in the glaze (Figure 3b). Semi-bubbles are visible on the surface of the glaze cross-section, as well as white spherical particles with blurred edges (Figure 4b). SEM imaging (taken with different acceleration voltages, 5 and 15 kV) revealed that these spherical particles are present inside the glaze, below the surface of the polished section (Figure S1). These particles, analyzed by SEM-EDS, are mainly rich in potassium, chlorine, and sulfur (Figure 4c). There are few data in the literature to explain the presence of these salts, which glassmakers call "bouillon de sels" or galle [18–21]. The semi-bubbles observed on the surface of the cross-section also most probably contained salts that were dissolved during the polishing stage. The sulfur and chlorine present in the glaze could be provided by natural ingredients such as plant ash [22]. The presence of these salts could indicate that a glazing mixture was deposited directly on the brick rather than using a colored frit. Regarding the coloring of this glaze and according to EDS analysis, it appeared that the dark color used for the colored field was achieved by adding manganese to the glass matrix (around 3 wt% MnO). Moreover, iron is also present in the glass matrix, in the order of 0.5 wt% Fe_2O_3. This coloring method is widespread in ancient glass and glazes: manganese in oxidation state +3 dissolved in the matrix can give a black hue [23].

Table 1. Average chemical composition of the glass matrix of different black glazes of Susa, measured by EDS analysis (wt% normalized to 100%). As a comparison, we indicate the average composition of ancient Mesopotamian glasses published in Shortland and Eremin (2006) [24]. Numbers in parenthesis indicate the standard variation and <LOQ signifies below quantification limit, *n* corresponds to the number of the glazes analyzed, and nd to non-detected.

	SiO_2	Al_2O_3	Na_2O	K_2O	CaO	MgO	Fe_2O_3	CuO	MnO	TiO_2	CoO	ZnO	SO_3	Cl
Flat glaze (n = 1)	89.0 (0.1)	0.4 (0.1)	0.3 (0.1)	0.7 (0.2)	2.8 (0.4)	0.4 (0.1)	0.5 (0.1)	nd	3.0 (0.1)	nd	nd	nd	1.3 (0.1)	1.6 (0.1)
Separating glazes (n = 3)	69.4 (1.4)	2.7 (0.6)	12.8 (0.6)	2.3 (0.3)	3.6 (0.7)	2.0 (0.3)	4.5 (1.4)	1.4 (1.0)	<LOQ	0.2 (0.1)	0.5 (0.6)	<LOQ	0.4 (0.1)	0.4 (0.2)
Ancient Mesopotamian glasses [24]	62.8	0.5	15.9	2.3	6.4	4.3	0.2	-	-	-	-	-	0.2	0.8

On the contrary, the black line separating glaze has a different morphology: the thick glaze forms a bulge (from one to several millimeters thick) to prevent adjoining flat glazes from fusing together during the firing (Figure 5a). Observation of glaze cross-sections revealed the presence of many particles of widely varying colors and sizes inside the glass matrix (Figures 3c and 5b). The most abundant part consists of transparent inclusions of a wide range of sizes (from several hundred microns to less than ten microns in length) dispersed in the glass matrix (Figure 5b,c). EDS and μ-Raman analyses identified quartz inclusions (SiO_2), probably unmelted particles. The angular shape of some quartz grains suggests that siliceous rocks (like quartz pebbles or quartzite) were coarsely crushed and added to the glazing mixture (Figure 5b). Other smaller quartz inclusions have blunt edges that indicate that there was a reaction between their surface and the liquid glaze at high temperature (Figure 5c). The large amount of quartz raises the melting temperature of this kind of black glaze compared to the other colors present on the brick. Moreover, the intentional adding of quartz increases significantly the apparent viscosity of the glaze and ensures that glazes adjacent to the contour lines do not mix together. Indeed, the presence of solid heterogeneities dispersed in a liquid glaze is known to induce an increase in the viscosity of the system due to an increase in the flow resistance [25]. A large number of bubbles of varying sizes, up to several hundred microns, is also noticeable in the glazes (Figures 3c and 5b). It would appear that the high viscosity of the glaze prevented the bubbles from escaping the molten liquid that trapped them. Other inclusions can also be seen, grayish in color and quite large in size (up to 50 μm, Figure 5b,c). These inclusions were identified thanks to SEM-EDS analysis as iron-bearing Ca-clinopyroxene inclusions (augite, $(Ca,Mg,Fe,Al)_2(Al,Si)_2O_6$)) (Figure S2). Supporting the EDS results, Raman bands centered at 323, 355, 390, 664 and 1007 cm^{-1} confirmed the presence of augite (Figure S2) [26]. Their morphology and size suggest that these crystallizations were initially present in the glaze mixture. Nevertheless, clinopyroxenes are found in magmatic rocks, and in the immediate geological environment of the city of Susa there are no magmatic rocks (such as basalt, for example). The use of magmatic rocks in the production of glazed bricks in Susa would therefore have led to long-distance trade, whereas we might have thought that another available material could replace it.

Black and red particles are also dispersed in the glass matrix. The size of the red grains varies between several dozen and a few microns (Figure 5b). Their observation by SEM revealed a very particular morphology with crystallization stripes of lighter contrast in the images (Figure 6a). Raman bands at 228, 247, 294, 413, 509, 609, 668, and 1324 cm^{-1} allowed us to identify hematite by comparison with the RRUFF database (Figure 6b) [27]. These lines of crystals seem to grow on an area that is particularly rich in magnesium (39.3 wt% MgO), silicon (39.0 wt% SiO_2), and iron (20.2 wt% Fe_2O_3). Surprisingly, the chemical composition of this area is very close to olivine $(Mg,Fe)_2SiO_4$. It is interesting to note that olivine is also known to occur in basaltic rocks, like augite. The olivine inclusions present in the glazes may have been transformed during glaze firing, leading to the formation of the

hematite that covers them [28]. Moreover, we observed, around the red particles, a border of neo-formed crystals rich in Ca, Na, and Si (Figure 6c, spectrum 3). These neo-formed crystals are most probably the result of the reaction during firing between the iron-rich inclusion and the glass matrix around it (Table 1).

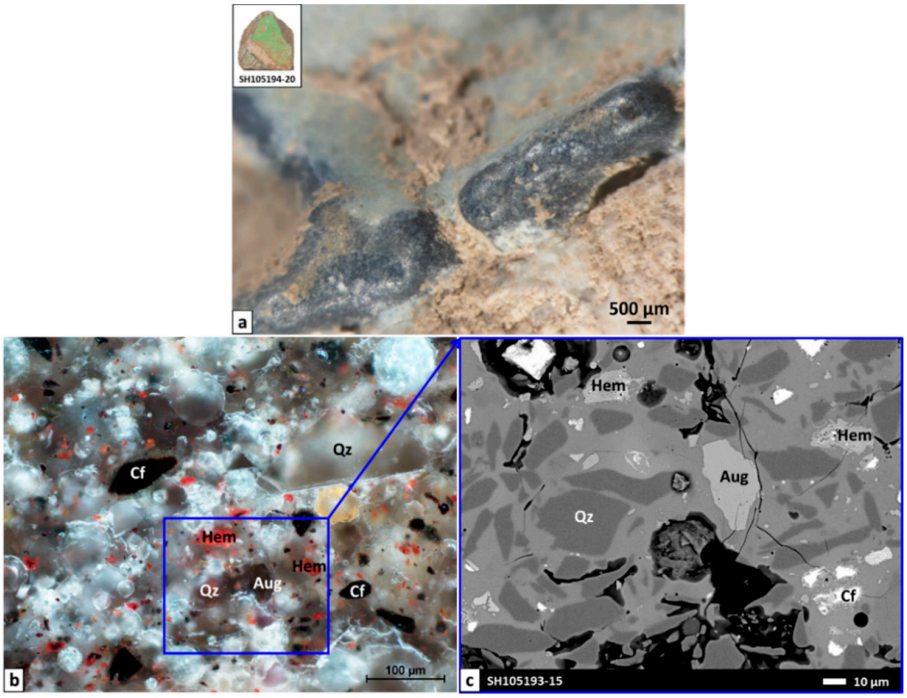

Figure 5. Optical microscope photographs of the surface (**a**) and the cross-section (**b**) of a Susa black raised line. The framed area in the SEM backscattered electron image (**c**) corresponds exactly to the same area as the photograph (**b**). Qz: quartz, Hem: hematite, Aug: augite, and Cf: cobalt ferrite.

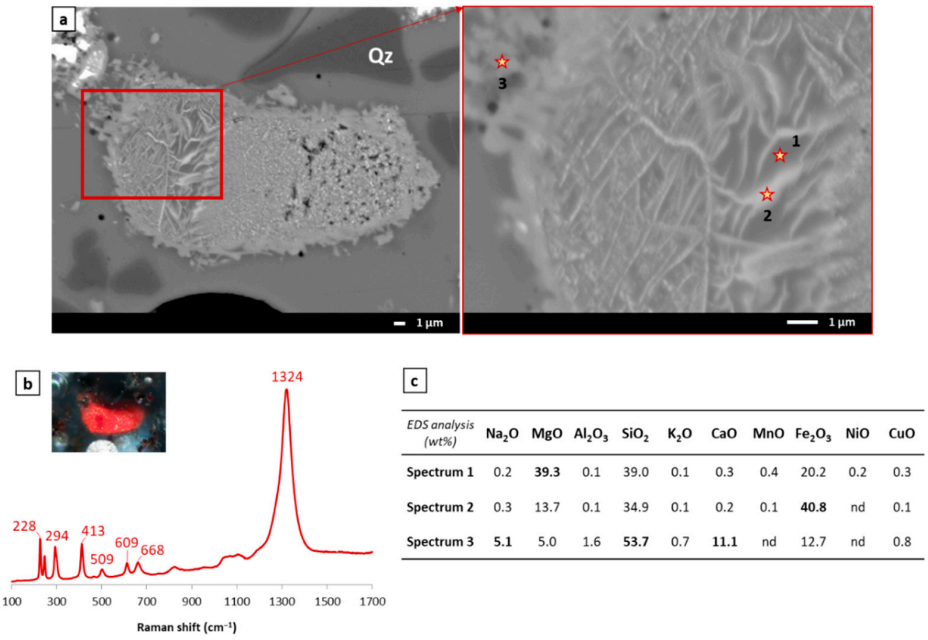

EDS analysis (wt%)	Na_2O	MgO	Al_2O_3	SiO_2	K_2O	CaO	MnO	Fe_2O_3	NiO	CuO
Spectrum 1	0.2	**39.3**	0.1	39.0	0.1	0.3	0.4	20.2	0.2	0.3
Spectrum 2	0.3	13.7	0.1	34.9	0.1	0.2	0.1	**40.8**	nd	0.1
Spectrum 3	**5.1**	5.0	1.6	**53.7**	0.7	**11.1**	nd	12.7	nd	0.8

Figure 6. (**a**) SEM backscattered electron images, (**b**) optical microscope photograph and µ-Raman spectrum of red particles present inside black separating glazes from Susa. (**c**) Chemical composition of different parts of a red particle present in the black separating glazes of Susa. Inset illustrated colored particle analyzed and the stars correspond to the EDS spots whose results are reported in (**c**). Qz = quartz; nd = non-detected.

Concerning the black inclusions, they are at least ten microns long (Figure 5b). The analysis by μ-Raman showed three bands centered at 325, 480, and 700 cm^{-1}, which can be attributed to cobalt ferrite ($CoFe_2O_4$) by comparison with the literature [29] (Figure 7a,b). Moreover, the EDS analysis highlighted high concentrations of copper (1.3 at%) and zinc (2.1 at%) (Figure 7c). Nickel is also found in quantities close to the detection limit (0.2 at%). These different elements were most certainly associated with cobalt in the raw materials used to color the glazes and could be markers of the raw materials used [30]. Moreover, it can be assumed that zinc and copper may have substituted for cobalt in the spinel ferrite structure [31,32]. Like augite and olivine, cobalt ore can be derived from magmatic rocks, since it is frequently formed by the leaching of cobalt from ultramafic rocks [33]. As we saw previously for red particles, there is a zone of crystallization between the glass matrix and the cobalt ferrite grain: we noticed a border of neo-formed crystals that mainly contain Ca, Na, Si, and some Fe (probably diffused from cobalt ferrite) (Figure 7c).

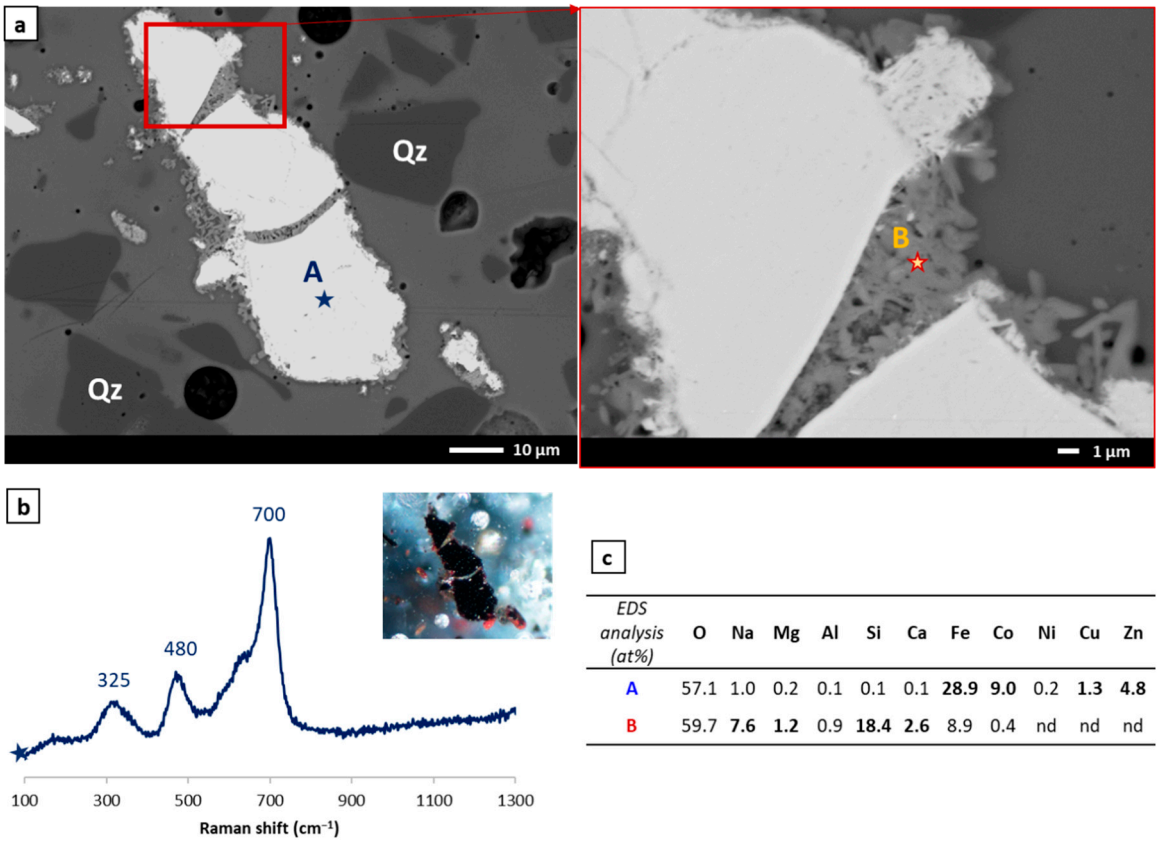

EDS analysis (at%)	O	Na	Mg	Al	Si	Ca	Fe	Co	Ni	Cu	Zn
A	57.1	1.0	0.2	0.1	0.1	0.1	**28.9**	**9.0**	0.2	**1.3**	**4.8**
B	59.7	**7.6**	**1.2**	0.9	**18.4**	**2.6**	8.9	0.4	nd	nd	nd

Figure 7. (**a**) SEM backscattered electron images, (**b**) optical microscope photograph, and μ-Raman spectrum of black particles present inside black separating glazes from Susa. (**c**) Chemical composition of different parts of a black particle present in the black separating glazes of Susa. Inset illustrated colored particle analyzed, and the stars correspond to the EDS spots whose results are reported in (**c**). Qz = quartz; nd = non-detected.

These different particles are dispersed in a glass matrix that appears to be unaltered, as shown by the amount of alkali present (approximately 15 wt% $Na_2O + K_2O$, Table 1). The amount of potassium and magnesium could suggest the use of plant ash [22]. In addition, it is interesting to note that the average composition of ancient Mesopotamian glasses is very close to the vitreous matrix of the black separating glaze (Table 1). The small and highly variable amounts of copper, cobalt, and iron detected in the glass matrix (1.4 wt% CuO, 0.5 wt% CoO, and 4.5 wt% Fe_2O_3 on average, Table 1) can be attributed to the diffusion of these elements from the colored iron, copper, and cobalt-rich particles present in the glazes. In conclusion, the dark color of this kind of glaze is mainly attributed to the presence of

black and red particles, but the glass matrix, which contains a significant amount of iron, copper, and cobalt, also contributes to the black color (Table 1).

3.2. Khorsabad Glazes

As at Susa, the black color is used both to draw the motifs' outline and to fill the colored fields (Figure 2a). However, unlike the Achaemenid bricks of Susa, the separating black glazes of Khorsabad do not show a specific relief-like bulge (Figure 8a,b). That is why, both on the surface of the bricks and on the sample cross-section, we can see that the limit between the different colored glazes is not clearly defined (Figure 8a,b). The thickness of all the glazes varies between 300 and 500 µm. In the following, we will first present the results obtained on black glazes not adjacent to a yellow glaze and then those concerning black glazes located close to a yellow glaze.

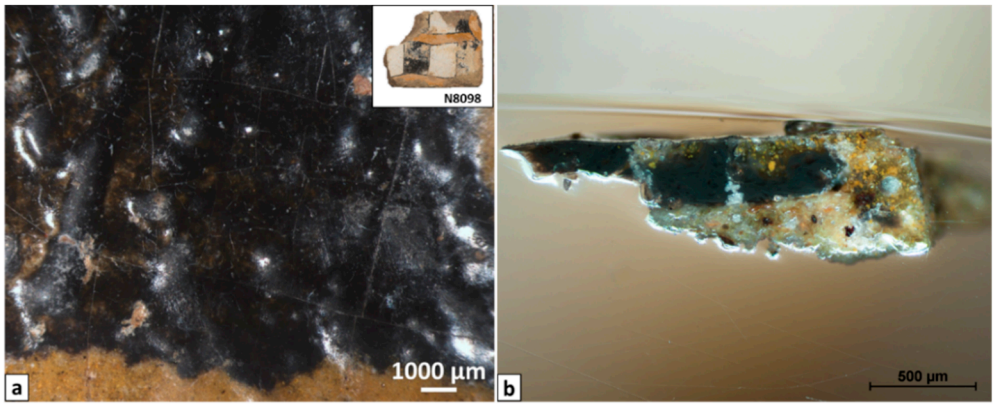

Figure 8. Optical microscope photographs of the surface (**a**) and the cross-section (**b**) of a black glaze close to a yellow glaze on a brick found at Khorsabad.

3.2.1. Study of Black Glazes Not Close to Yellow Glazes

Two samples from the brick N8123 (pr30 and pr31, Figure 2a) have the particularity of not being close to a yellow glaze. The cross-sections of these samples show a black appearance under optical microscopy (Figure 9a). By observing the cross-sections of these samples, we can distinguish dark volutes constituted of black particles suspended within the transparent glaze. The scattering of light by the nanoparticles explains the whitish color of the volutes (Figure 9b). Actually, SEM observation revealed that the black volutes are constituted of a large number of spherical nanoparticles dispersed in the glass matrix (Figure 9c,d). The size of these nanoparticles is very variable, ranging from less than 100 nm to about 1 µm for the larger ones. However, the large majority of particles are smaller than 500 nm (Figure 9d).

Some nanoparticles contained in samples pr30 and pr31 were probed by EDS spot analyses. Table S1 summarizes the chemical composition of some of the nanoparticles examined. It should be noted that, depending on the size of the nanoparticles, they contain more or less silica (which corresponds to the contribution of the glass matrix surrounding the particles). Compared to the glass matrix, the nanoparticles are especially rich in copper and sulfur (between 1.9 and 27.8 at% Cu and 0.9 and 12.6 at% S, Supplementary Material, Table S1) and the content of these two elements seems to be directly correlated. In fact, the stoichiometric ratio calculated between copper and sulfur might suggest that these nanoparticles consist of copper sulfide, probably as $Cu_{1.9}S$ (Figure 10a). This result was confirmed by X-ray diffraction analysis, which highlighted the presence of chalcocite (Cu_2S) in the two samples studied (pr30 and pr31) (Figure 10b).

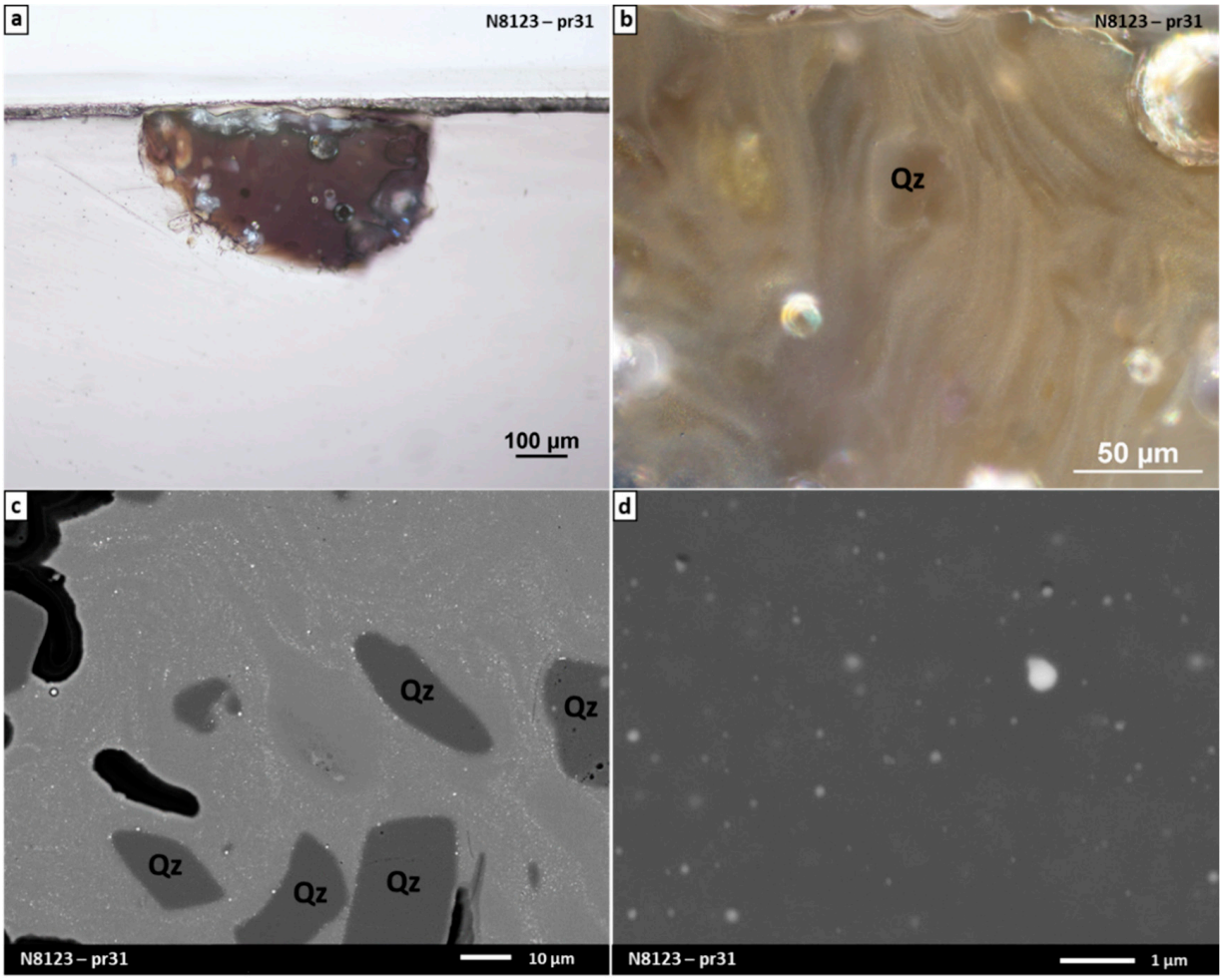

Figure 9. Microphotographs (**a**,**b**) and SEM backscattered electron images (**c**,**d**) of nanoparticles present inside isolated black glazes from Khorsabad (N8123, pr30 and pr31). Quartz (Qz) inclusions are visible in the glazes under both optical microscopy (white inclusions for (**a**) and transparent inclusions for (**b**) and SEM (**c**)). The scattering of light by the nanoparticles produces the white color of the volutes (**b**).

Furthermore, X-ray diffraction indicated the presence of quartz grains (SiO_2) visible in the optical microscopy and SEM images (Figure 9). Their size varies from about ten microns to about fifty microns in length (Figure 9c). The morphology of the quartz inclusions and their blunt edges indicate that there was a reaction between the surface of the particles and the liquid glaze at high temperature.

The relative intensity of the bands in the X-ray diagram demonstrated that the proportion of the Cu_2S crystalline phase is much lower than that of quartz. This observation confirms the optical microscopy and SEM images, which showed the presence of large quartz grains (Figure 9). In addition, SEM-EDS analysis also allowed us to assess the high quantity of copper sulfide nanoparticles present in the glaze.

The quartz inclusions and spherical particles are immersed in a vitreous matrix mostly composed of silica (SiO_2 contents higher than 70 wt%) and alkaline fluxes (between 13.5 and 15.8 wt%0 Na_2O and 3.1 and 3.5 wt% K_2O on average). Finally, we also noted the significant presence of calcium (between 4.5 and 5.6 wt% CaO) and the low content of SO_3 (0.4–0.8 wt%) (Table 2). It is interesting to highlight that no chromogenic elements were detected in the glass matrices of these two samples.

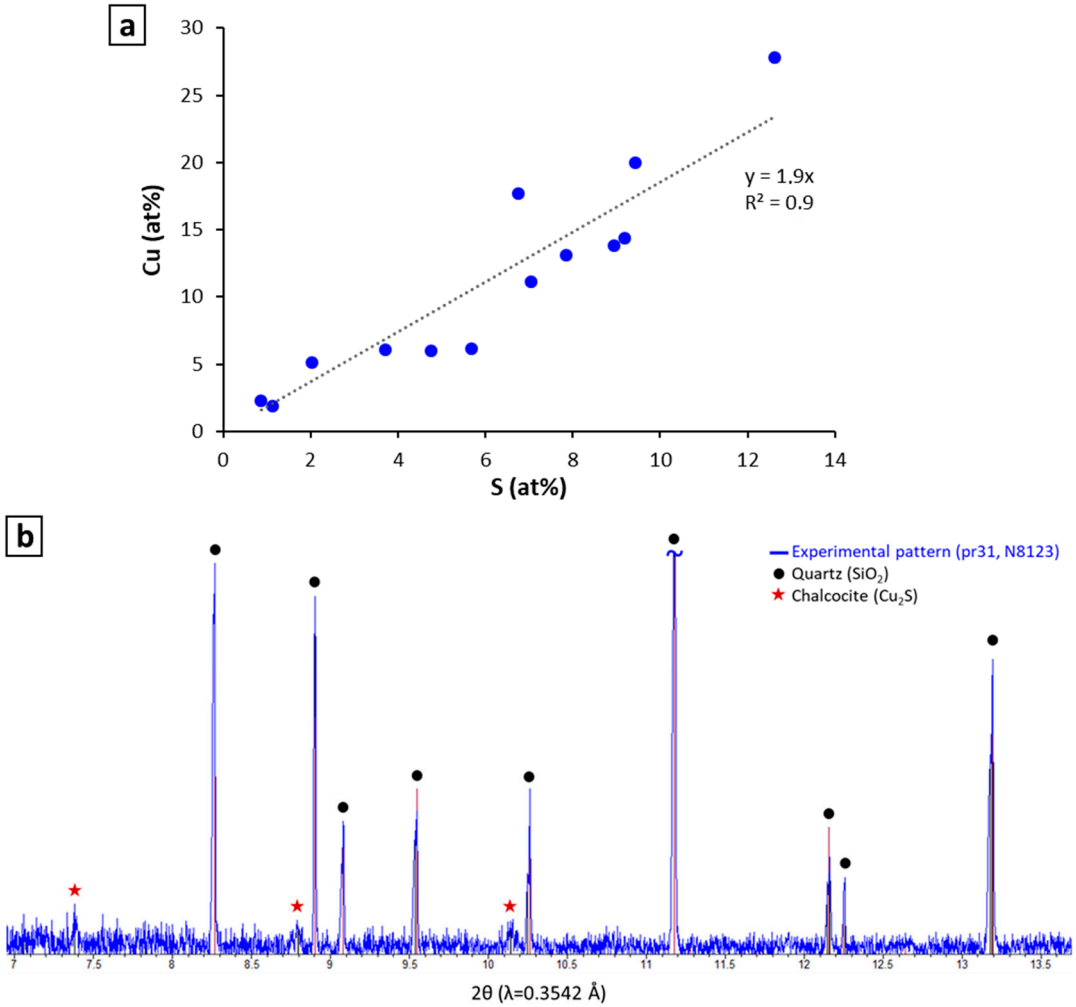

Figure 10. (**a**) Bivariate plots of Cu vs. S to compare the composition of different nanoparticles analyzed in the black isolated glazes from Khorsabad (pr30 and pr31, brick N8123). The chemical composition measured by EDS (at%) shows that the Cu and S contents vary proportionally (detailed elemental compositions of the analyzed nanoparticles are included as additional material in Table S1). (**b**) X-ray diffractogram of a representative sample of an isolated black glaze from Khorsabad (pr31, N8123).

Table 2. Average chemical composition of glass matrices of Khorsabad glazes, measured by EDS analysis (wt% normalized to 100%). *n* corresponds to number of analyzed glaze samples, nd indicates non-detected, and <LOQ signifies below quantification limit.

	SiO_2	Al_2O_3	Na_2O	K_2O	CaO	MgO	Fe_2O_3	CuO	TiO_2	Sb_2O_3	PbO	SO_3	Cl
N8123 pr30	70.2 (0.3)	1.9 (0.5)	15.8 (0.2)	3.1 (0.1)	4.5 (0.1)	2.6 (0.1)	0.7 (0.3)	0.2 (0.1)	0.1 (0.1)	nd	nd	0.8 (0.1)	0.1 (0.1)
N8123 pr31	71.3 (1.0)	1.6 (0.3)	14.0 (0.4)	3.5 (0.1)	5.6 (0.2)	2.6 (0.1)	0.5 (0.1)	0.3 (0.2)	<LOQ	nd	nd	0.4 (0.1)	0.4 (0.1)
Glass matrix of black glazes close to yellow color (*n* = 4)	71.7 (2.5)	1.4 (0.6)	13.5 (0.2)	3.3 (0.2)	4.6 (0.4)	2.4 (0.3)	0.9 (0.6)	0.1 (0.1)	0.2 (0.3)	**0.4 (0.5)**	**0.9 (1.0)**	0.7 (0.1)	0.2 (0.1)

3.2.2. Study of Black Glazes Close to a Yellow Glaze

The other samples of black glazes, which represent the main part of the corpus, are situated beside a yellow glaze. The limit between adjacent glazes, yellow area, and black line is not clearly defined; it remains a region where colored glazes mix together (Figure 11a). From the point of view of the color and the morphology of the glazes, there

are no significant differences between the two samples and black glazes described above, which are not located close to a yellow glaze. Observation of the glaze cross-sections by optical microscopy revealed the presence of dark volutes (Figure 11a) composed of black particles (appearing in white in Figure 11b). Actually, SEM observation indicated that the black volutes are constituted of a large number of nanoparticles dispersed in the glass matrix (Figure 11c,d). As we saw above, the size of these spherical nanoparticles is very variable, ranging from less than 100 nm to about 1 µm for the larger ones. Nevertheless, the great majority of particles are smaller than 500 nm. Unlike isolated black glazes, it should be noted that the contrasting SEM images indicated that the nanoparticles presented are not chemically homogeneous (Figure 11d,e). In fact, we observed this in nanoparticle regions richer in heavy elements (appearing in white on the SEM images), most often present on the edge of the particles (see arrows in Figure 11d). This morphology suggests that the phases have crystallized heterogeneously from the interface between the spherical droplet and the surrounding silicate phase.

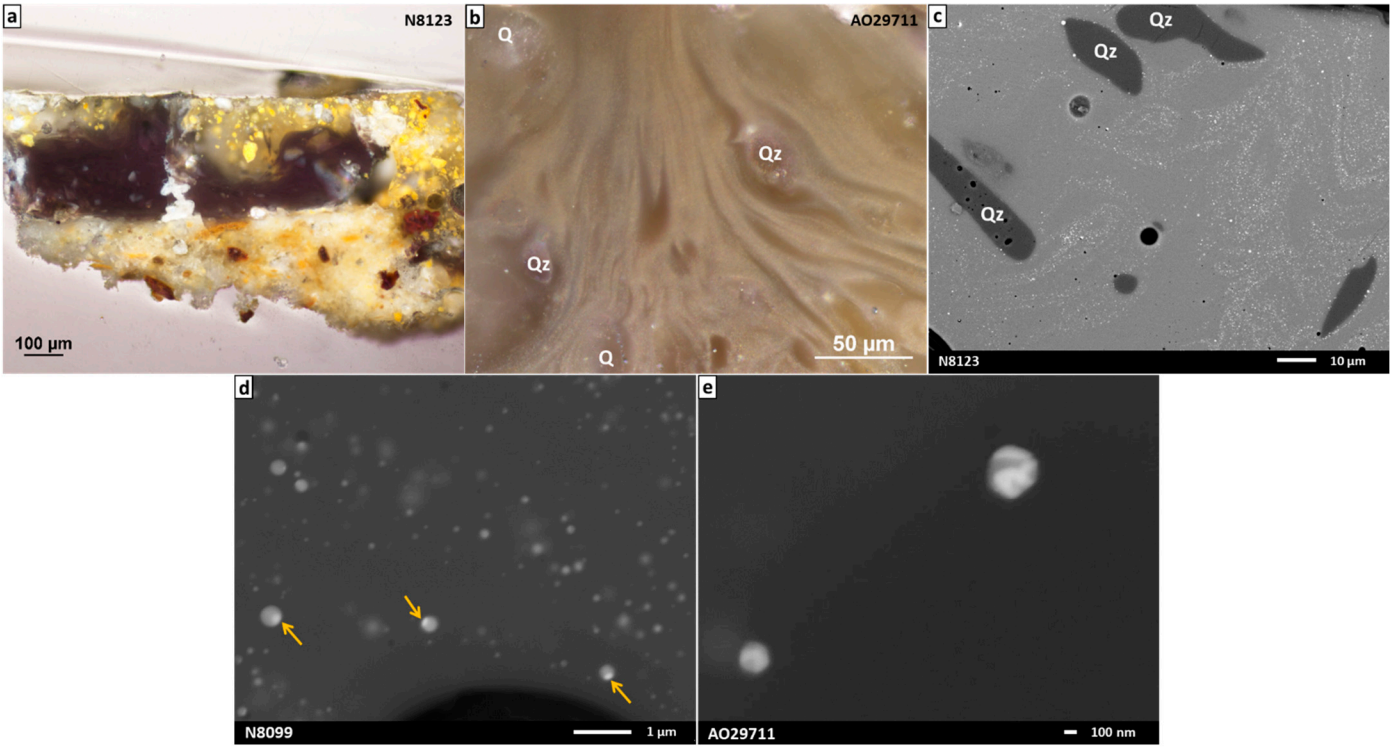

Figure 11. Microphotographs (**a**,**b**) and SEM backscattered electron images (**c**–**e**) of nanoparticles present inside black glazes located next to yellow glazes from Khorsabad. Here again we can distinguish quartz (Qz) inclusions under both optical microscopy (white inclusions for (**a**) and transparent inclusions for (**b**)) and SEM (**c**). The scattering of light by the nanoparticles produces a white color of the nanoparticles (**b**). The arrows present in (**d**) point to regions richer in heavy elements at the edge of the nanoparticles.

EDS spot analyses were carried out on the largest nanoparticles and demonstrated that two different regions coexist: one mainly composed of copper and sulfur (shown in gray on the SEM images) and the other rich in lead and sulfur (shown in white on the SEM images; Figure 12a,b). Two phases can be defined on the basis of EDS chemical analysis: phase A, enriched in lead ($Cu_{0.7}Pb_{0.6}S$), and phase B, richer in copper $Cu_{2.1}Pb_{0.1}S$ (Figure 12a,b). The small amount of lead in phase B is probably due to the contribution of phase A during spot analysis. In addition, other chemical elements like iron, silver, nickel, or antimony can be occasionally detected in low quantities in the particles. Concerning the significantly high content of SiO_2 (between 14 and 17 wt%), it can be attributed to the surrounding glass matrix (Figure 12b).

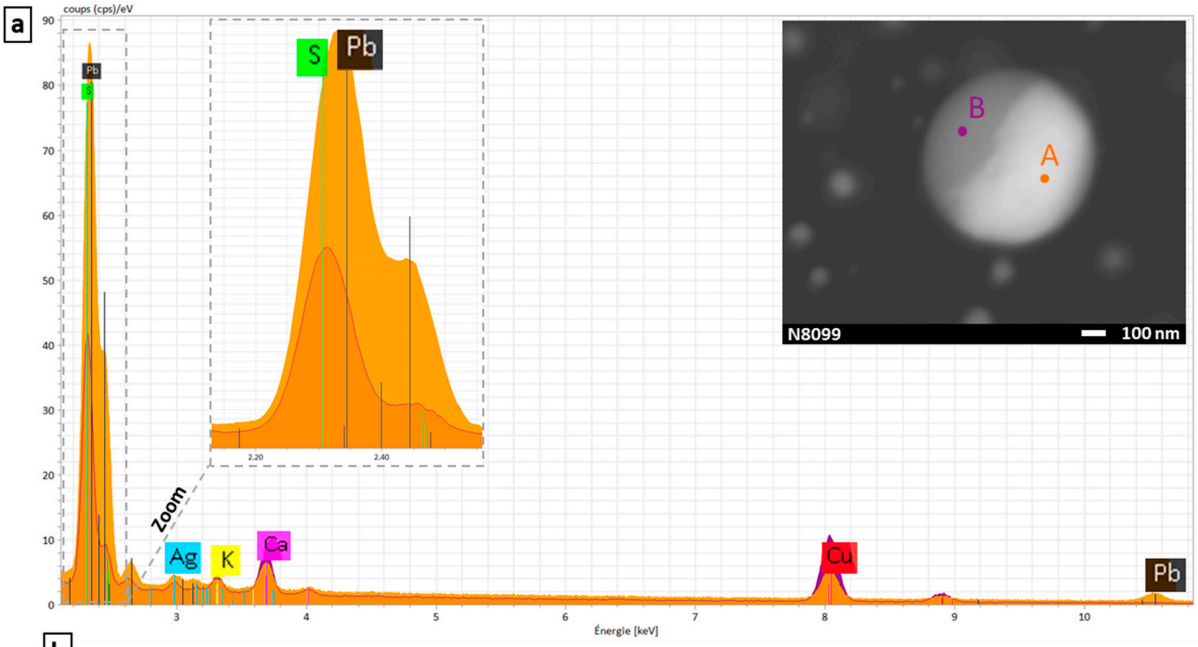

b

	O	Na	Mg	Al	Si	S	Cl	K	Ca	Fe	Cu	Ag	Pb
Spectrum A	64.2	0.9	1.1	0.4	14.0	**7.5**	0.1	0.2	1.1	0.1	5.3	0.3	**4.8**
Spectrum B	62.8	1.4	1.5	0.5	17.1	**4.6**	0.1	0.4	1.3	0.1	**9.6**	0.1	0.5

Figure 12. (**a**) EDS spectra and SEM backscattered electron image of the two areas of a nanoparticle present inside a black glaze from Khorsabad close to a yellow glaze (brick N8099); (**b**) detailed chemical compositions of each area (A and B) of the nanoparticle, measured by EDS analysis (at% normalized to 100%). The orange spectrum corresponds to region A and the purple spectrum corresponds to region B.

From a mineralogical point of view, SXRD analysis of the black glazes of the bricks AO29711 and N8080 indicated the presence of quartz (SiO_2), gypsum ($CaSO_4 \cdot 2H_2O$), and galena (PbS) (Figure S3). Galena was identified in a very small amount compared with other crystalline compounds. Unlike black glazes that are not close to a yellow glaze, chalcocite, which could correspond to phase B, was not detected by XRD. However, its presence can be assumed on the basis of SEM-EDS analyses. Compared with lead (Z = 82), copper (Z = 29) has a much lower atomic scattering factor, so the intensity of the copper sulfide diffraction peaks is lower than for lead sulfide. Therefore, galena is better detected in XRD than chalcocite. Gypsum could be considered as pollution from the soil environment during burial. As for isolated black glazes, quartz grains (probably unmelted particles initially present in the mixture deposited on the bricks before heating) with blunt edges are actually visible in the glass matrix. Their size varies between ten and fifty microns in length (Figure 11c).

Chemical EDS analysis of the glass matrix did not show any significant differences between black glazes sampled that were near a yellow glaze and those that were not, except concerning antimony and lead contents. In fact, it was observed that the soda-lime matrix close to a yellow glaze (colored by the addition of lead antimonates particles, $Pb_2Sb_2O_7$) contains both antimony and lead in small (respectively, 0.4 and 0.9 wt%, on average) and disparate amounts (as shown by the calculated standard deviations reported in Table 2). On the contrary, the matrix of the two isolated black glazes pr30 and pr31 do not contain antimony and lead at all (Table 2). That is why the presence of lead in the black nanoparticles and in the glass matrix can be explained by diffusion of this chemical element from the yellow glazes to the adjacent black glaze.

4. Discussion and Contextualization of the Production Techniques of the Black Glazed Bricks in the Middle East

The first use of dark separating colored glazes in architectural bricks was documented as early as the Elamite period (13th century BC) at Chogha Zanbil and Susa [6,34]. Thanks to the data already published in the literature, we drew up a table summarizing the processes used to produce a black glaze between the 13th and 4th centuries BC (Table 3). Thus, we can contextualize the data obtained in this study.

Previous work on Neo-Elamite glazed pieces found at Susa showed that dark separating glazes were especially rich in unmelted quartz and hematite inclusions that color the glass matrix [6]. This kind of recipe seems to have remained until the Persian Achaemenid period in Elam. Actually, studies on Achaemenid black contour glazes from Susa and Persepolis have shown the preponderance of iron-rich minerals (like hematite and/or magnetite) [3,4,17,35,36]. Nevertheless, some chemical elements have also been detected in these glazes, such as copper, which contributes to the dark appearance of the glaze. In addition, the Persepolis samples (Achaemenid Empire, mid-first millennium BC) are characterized by significant cobalt contents [3]. Several papers report the presence of a large number of quartz inclusions in the dark-colored relief glazes that heighten their melting point and viscosity and thus prevent the mixing of glazes between them [3,6,17,35]. As we have seen in the study of the black separating glaze of Susa, our results are in accordance with the results of previous studies [4,35]. We identified the high amount of hematite and quartz inclusions and determined from a mineralogical point of view in which form the cobalt is present (cobalt ferrite associated with high amounts of Cu and Zn). During the late antique period, cobalt colorants were associated with impurities such as iron, nickel, and copper (with occasionally zinc and lead). On the contrary, between the 8th and 12th centuries in the Islamic world, the use of a new type of zinc-rich source cobalt appeared [37]. Although it is difficult to deduce where the ore was extracted, it is interesting to note that in the case of the cobalt-rich particles present in the Susa glazes, the cobalt is mostly accompanied by iron, copper, and zinc. Moreover, it should be noticed that the Persepolis dark separating glazes contained cobalt that is probably associated with arsenic [3]. We also highlighted a clear modification in the recipes and coloring agents related to the use of the black glaze during the Persian Achaemenid period. As a matter of fact, the black coloration is obtained thanks to manganese oxide (for colored fields) and to iron-rich compounds (hematite and cobalt ferrite, for relief lines separating glazes). It is also noteworthy that manganese (associated with a high Fe concentration) was also identified in black glazes used for colored areas in the bricks of Nimrud (Neo-Assyrian period) [38,39]. From a more general point of view, it is important to mention that the use of manganese as a glass colorant has been highly developed and well-known since antiquity [23,40,41].

The Neo-Assyrian and Neo-Babylonian periods seem to be marked by another particular technology for the production of black glazes based on the presence of copper sulfide nanoparticles. Concerning the Khorsabad glazes examined in this study, it is interesting to note that we determined that whatever the function of the black glaze (contour line or colored field), the type of coloring of the glazes is the same. In fact, a further study reported the identification of nanoparticles rich in copper and sulfur that produced black color in ancient bricks [5]. The presence of sulfur and copper-rich nanoparticles has also been reported in several published papers concerning other dark archaeological glazes [21,42–45]. The use of this kind of coloration is attested to across a wide chronological and geographical range, for the black coloration of glass vessels and beads and also of glazed ceramics. Actually, this coloring method is described for productions from Iran, Iraq, and Jordan between the 2nd millennium BC and the 15th century AD. Stapleton and Swanson pointed out that in black glasses from Hasanlu (9th century), the black particles comprise mixed copper–iron–lead–antimony sulfides [21]. However, the chemical heterogeneity of these kinds of nanoparticles, i.e., the presence of a Pb-rich phase like galena, has never been clearly reported. As these various sulfides are not miscible in the crystalline state, the sulfide liquid drops that separated from the surrounding silicate glass may have cooled to form polyphase

aggregates, which explains the heterogeneous areas observed in nanoparticles [46,47]. The minor chemical elements (particularly Pb, Sb, and Ag) may be markers of the ore used. Nevertheless, our results also seem to demonstrate that the chemical heterogeneity of the nanoparticles could be explained by the diffusion of elements present in the yellow-orange adjacent glaze. Furthermore, it is not clearly established how these nanoparticles were formed (probably neo-formed phases from the glaze mixture to be determined) and how they persist during firing, as sulfides oxidize easily. It will be necessary to check with laboratory replicas as to whether the nanoparticles could be the remains of larger copper and lead sulfide particles. Nevertheless, their size (no larger than a micron) and spherical shape suggest a formation in the glaze. Moreover, questions remain about the presence of these sulfide nanoparticles since their formation necessarily requires reducing conditions (probably obtained by means of the furnace atmosphere or/and by adding a reduced agent). The presence of turquoise (colored by Cu^{2+} dissolved in the glass matrix) and yellow glazes positioned on the same brick as the black glaze (Figure 2) implies that the glazed bricks were fired in an oxidizing atmosphere. From an economic point of view, it is more advantageous to fire all the glazes at the same time than to carry out a preliminary firing for the black contours and then another for the other colored glazes. Thus, several hypotheses can be formulated concerning the formation of these sulfides in the black glaze. The use of copper sulfide ores in the initial recipe is often proposed [21,38,42], especially as they had been employed in Mesopotamia for bronze metallurgy since the late Bronze Age [48]. Based on the study of Hasanlu green glazes (9th century BC), Holakooei et al. considered that the copper carrier of Mesopotamian glazes was provided by copper sulfide [38]. Another study suggests that the important thickness of the glaze (up to 650 µm and 1.3 mm) could be sufficient to prevent diffusion of oxygen and to explain the survival of copper sulfide particles [42]. The addition of an ingredient that would play the role of a reducing agent, such as charcoal or bitumen, is also possible. Bitumen could have been employed, particularly since it was commonly used at that time in the Middle East as an adhesive [49,50]. On the other hand, the black glaze may have required a preliminary preparation including a firing in a reducing atmosphere and then a final firing in an oxidizing condition with the other colors on the bricks. In order to understand the thermal protocols and the recipes that the ancient craftsmen could have followed to obtain the sulfide particles' presence, laboratory replicas have been implemented and the results will be presented in a forthcoming paper. At the same time, some studies on red glasses reported the presence of copper sulfide spherical particles and may allow us to better understand their formation [51–55].

Table 3. Summary of the black glazes used to decorate bricks in the Middle East between the 13th and 4th centuries BC.

Location	Period	Type of Glaze	Coloring Element	Nature of Colored Crystalline Phases	Other Phases Present	Chemical Composition of the Glass Matrix	Published Paper
Susa	Neo-Elamite (1000–539 BC)	Separating glaze	Fe	Hematite	Quartz	-	[6]
Khorsabad	Neo-Assyrian (900–610 BC)	Separating glaze + colored field		Copper sulfide nanoparticles + chromophore Fe^{3+}-S^{2-}	-	Soda–lime matrix	[5]
Nimrud	Neo-Assyrian (900–610 BC)	Colored field	Mn, Fe	Mn_2O_3, Mn_3O_4, $Mn(IV)_{1-2x}Mn(III)_{2x}O_{2-x}$	-	-	[38]
Nimrud	Neo-Assyrian (900–610 BC)	-	Mn (+Fe)	-	-	Soda–lime matrix	[39]
Tepe Rabat	8th–7th BC	Separating glaze	Fe, Cu	Hematite	Lead antimonate	-	[3]
Babylon	Neo-Babylonian (626–539 BC)	Separating glaze + colored field		Copper sulfide nanoparticles + chromophore Fe^{3+}-S^{2-}	-	Soda–lime matrix	[5]
Persepolis	Persian Achaemenid (539–330 BC)	Separating glaze	Co, Cu, Fe	Hematite, magnetite	Quartz	-	[3]

Table 3. *Cont.*

Location	Period	Type of Glaze	Coloring Element	Nature of Colored Crystalline Phases	Other Phases Present	Chemical Composition of the Glass Matrix	Published Paper
Persepolis	Persian Achaemenid (539–330 BC)	Separating glaze	Fe, Cu	Fayalite coated iron oxide, copper-bearing Mg-silicate	Quartz, calcite	-	[17]
Persepolis	Persian Achaemenid (539–330 BC)	Separating glaze (grayish)	Fe, Cu	-	-	-	[36]
Susa	Persian Achaemenid (539–330 BC)	Separating glaze	Fe, Cu	Hematite, magnetite	-	Alkali matrix	[4]
Susa	Persian Achaemenid (539–330 BC)	Separating glaze	Fe, Cu	-	Quartz	Alkali matrix	[35]

- no specific information is provided.

5. Conclusions and Future Works

In this paper, we investigated the black glazes of polychrome glazed bricks found in the Neo-Assyrian and Persian Achaemenid royal palaces. The well-preserved glazes of 13 colored bricks representative of the decoration of the palaces of Sargon II (Khorsabad, 8th century BC) and Darius I (Susa, 6th century BC) were examined using a combination of methods that included optical microscopy, SEM-EDX, synchrotron μ-XRD, and μ-Raman spectroscopy.

The results revealed major differences in the coloring techniques of black glazes employed in the Neo-Assyrian and Persian Achaemenid periods. Interestingly, we noted that the chemical composition of the black glazes of Susa varies according to the function of the glazes. In fact, the black coloration is obtained thanks to manganese oxide (for colored areas) and to iron-rich compounds (hematite and cobalt ferrite, for relief lines separating glazes). On the contrary, Khorsabad seems to be an exception as regards coloring techniques: the black color is characterized by the presence of copper sulfide and galena nanoparticles. For the first time, to our knowledge, we were able to demonstrate the chemical heterogeneity of the nanoparticles present in this dark decoration. We have especially shown that the presence of yellow glazes close to black glazes had an impact on the chemical composition of the latter due to probable diffusion between the two glazes. This coloring technique is very rarely described in the literature, as well as the mechanism of formation of these nanoparticles. Their spherical shape suggests that the formation of these crystalline phases was preceded by the formation of liquid particles, which then crystallized during cooling, possibly with successive sulfide crystallizations. Forthcoming research will focus on understanding how such microstructures could be obtained by forming a colored glass synthesis. Glazes produced under controlled conditions with different copper vectors and the presence (or not) of a reducing agent can give us some indications of the production techniques (recipes, firing temperature, and kiln atmosphere). Additional experiments in the laboratory should allow us to understand the conditions of elaboration of the glazes applied on the bricks and the production process. The effects of these parameters are currently under study and will be discussed in a forthcoming paper.

Supplementary Materials: The following supporting information can be downloaded at: https://www.mdpi.com/article/10.3390/heritage6090329/s1, Table S1. Chemical composition of some nanoparticles present in the isolated black glazes and separating lines of the two samples pr30 and pr31 as determined by EDS analysis (at%). nd indicates non-detected and <LOQ signifies below quantification limit. Figure S1. SEM backscattered electron images for two accelerating voltages of the black area from Susa (brick SB21474). Figure S2. (a) Optical microscope photograph. (b) Raman spectrum and (c) average chemical composition of an inclusion of augite present in the black separating glazes of Susa (Figure 5b,c). Figure S3. X-ray diffractogram of a representative sample of black glazes close to a yellow one (brick AO29711 from Khorsabad).

Author Contributions: Conceptualization, A.B., O.M., J.C. and A.T.; methodology, A.B., O.M., D.C. and E.B.; formal analysis, E.B.; investigation, E.B.; resources, J.C. and A.T.; data curation, E.B.; writing—original draft preparation, E.B.; writing—review and editing, A.B., O.M., D.C., J.C. and E.B.; visualization, E.B.; supervision, A.B., O.M. and D.C.; project administration, A.B.; funding acquisition, A.B., O.M., J.C. and A.T. All authors have read and agreed to the published version of the manuscript.

Funding: This work has benefited from state aid managed by the Agence Nationale de la Recherche (French National Research Agency) under the future investment program integrated into France 2030, reference ANR-17-EURE-0021—École Universitaire de Recherche Paris Seine Humanités, Création, Patrimoine—Fondation des Sciences du Patrimoine. The ESRF beamtime was granted through the peer-reviewed BAG proposal HG-172 at ID22. The Historical Materials BAG was implemented with support from the European Union's Horizon 2020 research and innovation program under grant agreement No 870313, Streamline.

Data Availability Statement: The data generated in this study is available upon request from the corresponding author.

Acknowledgments: The authors wish to thank the Fondation des Sciences du Patrimoine for its financial support through the ABRIKHOS project. We would also like to thank the European Synchrotron Research Facility (ESRF) for providing beamtime through the Historical Materials BAG (HG172) as well as Catherine Dejoie for her help with the use of the beamline ID22 and Marine Cotte, Victor Gonzales, Frederik Vanmeert, and Letizia Monico, scientists responsible for the Historical Materials BAG for their support of the program. The authors would like to warmly thank our colleagues Yvan Coquinot and Patrice Lehuédé for our fruitful discussions. We are also grateful to anonymous reviewers for their valuable comments and suggestions on the manuscript that helped to improve this paper.

Conflicts of Interest: The authors declare no conflict of interest.

References

1. Holakooei, P. Scientific Research on the Iron Age Glazes from Iran and Iraq: Past and Future. In *Glazed Brick Decoration in the Ancient Near East: Proceedings of a Workshop at the 11th International Congress of the Archaeology of the Ancient Near East (Munich) in April 2018*; Fügert, A., Gries, H., Eds.; Archaeopress Archaeology; Archaeopress Publishing Ltd.: Oxford, UK, 2020; pp. 16–28. ISBN 978-1-78969-605-9.
2. Fügert, A.; Gries, H. 'I Had Baked Bricks Glazed in Lapis Lazuli Color'1–A Brief History of Glazed Bricks in the Ancient Near East. In *Glazed Brick Decoration in the Ancient Near East: Proceedings of a Workshop at the 11th International Congress of the Archaeology of the Ancient Near East (Munich) in April 2018*; Fügert, A., Gries, H., Eds.; Archaeopress Archaeology; Archaeopress Publishing Ltd.: Oxford, UK, 2020; pp. 1–15. ISBN 978-1-78969-605-9.
3. Holakooei, P.; Ahmadi, M.; Volpe, L.; Vaccaro, C. Early Opacifiers In The Glaze Industry Of First Millennium BC Persia: Persepolis And Tepe Rabat: Early Opacifiers in First Millennium BC Persia. *Archaeometry* **2017**, *59*, 239–254. [CrossRef]
4. Holakooei, P. A Multi-Spectroscopic Approach to the Characterization of Early Glaze Opacifiers: Studies on an Achaemenid Glazed Brick Found at Susa, South-Western Iran (Mid-First Millennium BC). *Spectrochim. Acta Part A Mol. Biomol. Spectrosc.* **2013**, *116*, 49–56. [CrossRef] [PubMed]
5. Alloteau, F.; Majérus, O.; Gerony, F.; Bouquillon, A.; Doublet, C.; Gries, H.; Fügert, A.; Thomas, A.; Wallez, G. Microscopic-Scale Examination of the Black and Orange–Yellow Colours of Architectural Glazes from Aššur, Khorsabad and Babylon in Ancient Mesopotamia. *Minerals* **2022**, *12*, 311. [CrossRef]
6. Holakooei, P. A Technological Study of the Elamite Polychrome Glazed Bricks at Susa, South-Western Iran: Elamite Polychrome Glazed Bricks at Susa, South-Western Iran. *Archaeometry* **2014**, *56*, 764–783. [CrossRef]
7. McCarthy, J.; Paynter, S.; Tite, M.S.; Shortland, A.J. Production of glazed pottery and brickwork in the near east. In *Production Technology of Faience and Related Early Vitreous Materials*; Oxford University School of Archaeology: Oxford, UK, 2008; pp. 187–198.
8. Amadori, M.L.; Matin, E.; Poldi, G.; Mengacci, V.; Arduini, J.; Callieri, P.; Askari Chaverdi, A.; Holakooei, P. Archaeometric Research on Decorated Bricks of Tol-e Ajori Monumental Gate (6th Century BC), Fars, Iran: New Insight into the Glazes. *J. Cult. Herit.* **2023**, *60*, 63–71. [CrossRef]
9. Thomas, A. Glazed Bricks by the Dozens: A Khorsabad Jigsaw Reassembled at the Louvre. In *Glazed Brick Decoration in the Ancient Near East: Proceedings of a Workshop at the 11th International Congress of the Archaeology of the Ancient Near East (Munich) in April 2018*; Fügert, A., Gries, H., Eds.; Archaeopress Archaeology; Archaeopress Publishing Ltd.: Oxford, UK, 2020; pp. 48–84. ISBN 978-1-78969-605-9.
10. Thomas, A. Un puzzle en briques émaillées de Khorsabad. *Rev. D'assyriologie Et D'archéologie Orient.* **2020**, *114*, 103–158. [CrossRef]
11. Caubet, A.; Kaczmarczyk, A. Les briques glaçurées du palais de Darius. *Technè* **1998**, *7*, 23–26.

12. Caubet, A. Achaemenid Brick Decoration. In *The Royal City of Susa: Ancient Near Eastern Treasures in the Louvre*; Harper, P.O., Aruz, J., Tallon, F., Eds.; Metropolitan Museum of Art, Distributed by H.N. Abrams: New York, NY, USA, 1992; pp. 223–241. ISBN 978-0-87099-651-1.
13. Caubet, A. De l'Égypte à Suse, à propos de faïences perses achéménides. *Monum. Et Mémoires De La Fond. Eugène Piot* **2009**, *88*, 5–27. [CrossRef]
14. Shebanova, O.N.; Lazor, P. Raman Study of Magnetite (Fe_3O_4): Laser-Induced Thermal Effects and Oxidation. *J. Raman Spectrosc.* **2003**, *34*, 845–852. [CrossRef]
15. Cotte, M.; Gonzalez, V.; Vanmeert, F.; Monico, L.; Dejoie, C.; Burghammer, M.; Huder, L.; de Nolf, W.; Fisher, S.; Fazlic, I.; et al. The "Historical Materials BAG": A New Facilitated Access to Synchrotron X-Ray Diffraction Analyses for Cultural Heritage Materials at the European Synchrotron Radiation Facility. *Molecules* **2022**, *27*, 1997. [CrossRef]
16. Cotte, M.; Dollman, K.; Fernandez, V.; Gonzalez, V.; Vanmeert, F.; Monico, L.; Dejoie, C.; Burghammer, M.; Huder, L.; Fisher, S.; et al. New Opportunities Offered by the ESRF to the Cultural and Natural Heritage Communities. *Synchrotron Radiat. News* **2022**, *35*, 3–9. [CrossRef]
17. Raith, M.M.; Abdali, N.; Yule, P.A. Petrochemical Attributes of Glazed Architectural Elements from Middle-Elamite to Achaemenid Excavation Sites in Iran. *Archaeol. Anthropol. Sci.* **2022**, *14*, 182. [CrossRef]
18. Tanimoto, S.; Rehren, T. Interactions between Silicate and Salt Melts in LBA Glassmaking. *J. Archaeol. Sci.* **2008**, *35*, 2566–2573. [CrossRef]
19. Bontemps, G. *Guide du Verrier: Traité Historique et Pratique de la Fabrication des Verres, Cristaux, Vitraux*; Librairie du Dictionnaire des Arts et Manufactures: Paris, France, 1868.
20. Turner, W.E.S. Studies in Ancient Glasses and Glassmaking Processes. Part V. Raw Materials and Melting Processes. *J. Soc. Glass Technol.* **1956**, *40*, 277–300.
21. Stapleton, C.P.; Swanson, S.S. Batch Material Processing and Glassmaking Technology of 9th Century B.C. Artifacts Excavated from the Site of Hasanlu, Northwest Iran. *MRS Proc.* **2002**, *712*, II7.4. [CrossRef]
22. Tite, M.S.; Shortland, A.; Maniatis, Y.; Kavoussanaki, D.; Harris, S.A. The Composition of the Soda-Rich and Mixed Alkali Plant Ashes Used in the Production of Glass. *J. Archaeol. Sci.* **2006**, *33*, 1284–1292. [CrossRef]
23. Möncke, D.; Papageorgiou, M.; Winterstein-Beckmann, A.; Zacharias, N. Roman Glasses Coloured by Dissolved Transition Metal Ions: Redox-Reactions, Optical Spectroscopy and Ligand Field Theory. *J. Archaeol. Sci.* **2014**, *46*, 23–36. [CrossRef]
24. Shortland, A.J.; Eremin, K. The Analysis of Second Millennium Glass from Egypt and Mesopotamia, Part 1: New WDS Analyses. *Archaeometry* **2006**, *48*, 581–603. [CrossRef]
25. Liu, Z.; Pandelaers, L.; Blanpain, B.; Guo, M. Viscosity of Heterogeneous Silicate Melts: A Review. *Met. Mater. Trans. B* **2018**, *49*, 2469–2486. [CrossRef]
26. Sharma, S.K.; Angel, S.M.; Ghosh, M.; Hubble, H.W.; Lucey, P.G. Remote Pulsed Laser Raman Spectroscopy System for Mineral Analysis on Planetary Surfaces to 66 Meters. *Appl. Spectrosc.* **2002**, *56*, 699–705. [CrossRef]
27. Mineralogical Data on Hematite (Fe_2O_3), RRUFF ID: R050300. Available online: https://rruff.info/hematite/display=default/R050300 (accessed on 27 December 2021).
28. Gualtieri, A.F.; Gemmi, M.; Dapiaggi, M. Phase Transformations and Reaction Kinetics during the Temperature-Induced Oxidation of Natural Olivine. *Am. Mineral.* **2003**, *88*, 1560–1574. [CrossRef]
29. Wang, T.; Zhu, T.; Brunet, M.; Deshayes, C.; Sciau, P. Raman Study of Yuan Qinghua Porcelain: The Highlighting of Dendritic $CoFe_2O_4$ Crystals in Blue Decorations. *J. Raman Spectrosc.* **2017**, *48*, 267–270. [CrossRef]
30. Abe, Y.; Harimoto, R.; Kikugawa, T.; Yazawa, K.; Nishisaka, A.; Kawai, N.; Yoshimura, S.; Nakai, I. Transition in the Use of Cobalt-Blue Colorant in the New Kingdom of Egypt. *J. Archaeol. Sci.* **2012**, *39*, 1793–1808. [CrossRef]
31. Mameli, V.; Musinu, A.; Ardu, A.; Ennas, G.; Peddis, D.; Niznansky, D.; Sangregorio, C.; Innocenti, C.; Thanh, N.T.K.; Cannas, C. Studying the Effect of Zn-Substitution on the Magnetic and Hyperthermic Properties of Cobalt Ferrite Nanoparticles. *Nanoscale* **2016**, *8*, 10124–10137. [CrossRef] [PubMed]
32. Kamta Tedjieukeng, H.M.; Tsobnang, P.K.; Fomekong, R.L.; Etape, E.P.; Joy, P.A.; Delcorte, A.; Lambi, J.N. Structural Characterization and Magnetic Properties of Undoped and Copper-Doped Cobalt Ferrite Nanoparticles Prepared by the Octanoate Coprecipitation Route at Very Low Dopant Concentrations. *RSC Adv.* **2018**, *8*, 38621–38630. [CrossRef]
33. Ziwa, G.; Crane, R.; Hudson-Edwards, K.A. Geochemistry, Mineralogy and Microbiology of Cobalt in Mining-Affected Environments. *Minerals* **2020**, *11*, 22. [CrossRef]
34. Ghirshman, R. *Tchoga Zanbil (Dur-Untash). La Ziggurat*; Mémoires de la Délégation archéologique en Iran. Mission de Susiane; P. Geuthner: Paris, France, 1966; Volume XXIX.
35. Razmjou, S.; Tite, M.S.; Shortland, A.J.; Jung, M.; Hauptman, A. Glazed Bricks in the Achaemenid Period. In *Persiens Antike Pracht*; Stoellner, T., Slotta, R., Vatandoust, R., Eds.; Deutsches Bergbau-Museum: Bochum, Germany, 2004; pp. 382–393.
36. Aloiz, E.; Douglas, J.G.; Nagel, A. Painted Plaster and Glazed Brick Fragments from Achaemenid Pasargadae and Persepolis, Iran. *Herit. Sci.* **2016**, *4*, 3. [CrossRef]
37. Gratuze, B.; Pactat, I.; Schibille, N. Changes in the Signature of Cobalt Colorants in Late Antique and Early Islamic Glass Production. *Minerals* **2018**, *8*, 225. [CrossRef]
38. Holakooei, P.; Soldi, S.; de Lapérouse, J.-F.; Carò, F. Glaze Composition of the Iron Age Glazed Ceramics from Nimrud, Hasanlu and Borsippa Preserved at The Metropolitan Museum of Art. *J. Archaeol. Sci. Rep.* **2017**, *16*, 224–232. [CrossRef]

39. Freestone, I.C. Technical Examination of Neo-Assyrian Glazed Wall Plaques. *Iraq* **1991**, *53*, 55. [CrossRef]
40. Molera, J.; Coll, J.; Labrador, A.; Pradell, T. Manganese Brown Decorations in 10th to 18th Century Spanish Tin Glazed Ceramics. *Appl. Clay Sci.* **2013**, *82*, 86–90. [CrossRef]
41. Peix Visiedo, J.; Madrid i Fernández, M.; Buxeda i Garrigós, J. The Case of Black and Green Tin Glazed Pottery from Barcelona between 13th and 14th Century: Analysing Its Production and Its Decorations. *J. Archaeol. Sci. Rep.* **2021**, *38*, 103100. [CrossRef]
42. Ting, C.; Lichtenberger, A.; Raja, R. The Technology and Production of Glazed Ceramics from Middle Islamic Jerash, Jordan. *Archaeometry* **2019**, *61*, 1296–1312. [CrossRef]
43. Freestone, I.C.; Stapleton, C.P. Composition, technology and production of coloured glasses from Roman mosaic vessels. In *Glass of the Roman World*; Bayley, J., Freestone, I., Jackson, C., Eds.; Oxbow Books: Oxford, UK, 2015; pp. 61–76. ISBN 978-1-78925-339-9.
44. Kirk, S. The Vitreous Materials from the 2nd Millennium BC City of Nuzi: Their Preservation, Technology and Distribution. Ph.D. Thesis, Cranfield University, Cranfield, UK, 2009.
45. Mason, R.B.; Tite, M.S. The Beginnings of Tin-Opacification of Pottery Glazes. *Archaeometry* **1997**, *39*, 41–58. [CrossRef]
46. Tesfaye, F.; Taskinen, P. *Phase Equilibria and Thermodynamics of the System Zn-As-Cu-Pb-S at Temperatures Below 1173 K*; SCIENCE + TECHNOLOGY; Aalto University Publication: Helsinki, Finland, 2011; ISBN 978-952-60-4126-1.
47. Johto, H.; Taskinen, P. Phase Stabilities and Thermodynamic Assessment of the System Cu–Pb–S. *Miner. Eng.* **2013**, *42*, 68–75. [CrossRef]
48. De Ryck, I.; Adriaens, A.; Adams, F. An Overview of Mesopotamian Bronze Metallurgy during the 3rd Millennium BC. *J. Cult. Herit.* **2005**, *6*, 261–268. [CrossRef]
49. Schwartz, M.; Hollander, D. Annealing, Distilling, Reheating and Recycling: Bitumen Processing in the Ancient Near East. *Paleo* **2000**, *26*, 83–91. [CrossRef]
50. Connan, J. *Le Bitume dans l'Antiquité*; Editions Errance: Arles, France, 2012; ISBN 978-2-87772-504-0.
51. Arletti, R.; Ciarallo, A.; Quartieri, S.; Sabatino, G.; Vezzalini, G. Archaeometric Analyses of Game Counters from Pompeii. *Geol. Soc. Lond. Spec. Publ.* **2006**, *257*, 175–186. [CrossRef]
52. Andreescu-Treadgold, I.; Henderson, J. Glass from the Mosaics on the West Wall of Torcello's Basilica. *Arte Mediev.* **2006**, *5*, 87–140.
53. van der Werf, I.; Mangone, A.; Giannossa, L.C.; Traini, A.; Laviano, R.; Coralini, A.; Sabbatini, L. Archaeometric Investigation of Roman Tesserae from Herculaneum (Italy) by the Combined Use of Complementary Micro-Destructive Analytical Techniques. *J. Archaeol. Sci.* **2009**, *36*, 2625–2634. [CrossRef]
54. Santagostino Barbone, A.; Gliozzo, E.; D'Acapito, F.; Memmi Turbanti, I.; Turchiano, M.; Volpe, G. The Sectilia Panels of Faragola (Ascoli Satriano, Southern Italy): A Multi-Analytical Study of the Red, Orange and Yellow Glass Slabs. *Archaeometry* **2008**, *50*, 451–473. [CrossRef]
55. Yuan, M.; Bonet, J.; Cotte, M.; Schibille, N.; Gratuze, B.; Pradell, T. The Role of Sulphur in the Early Production of Copper Red Stained Glass. *Ceram. Int.* **2023**, *49*, 18602–18613. [CrossRef]